Experimental Model of Far Temporal Field Negative Dysphotopsia Generated in Phakic Eyes

Viswanathan Ramasubramanian, Dawn Meyer, Pete S. Kollbaum, and Arthur Bradley

Indiana University School of Optometry, Bloomington, Indiana, United States

Correspondence: Viswanathan Ramasubramanian, Indiana University School of Optometry, 800 E. Atwater Avenue, Bloomington, IN 47405, USA;
viswa.gr@gmail.com.

Received: February 21, 2020
Accepted: April 8, 2020
Published: May 16, 2020

Citation: Ramasubramanian V, Meyer D, Kollbaum PS, Bradley A. Experimental model of far temporal field negative dysphotopsia generated in phakic eyes. *Invest Ophthalmol Vis Sci.* 2020;61(5):24. https://doi.org/10.1167/iovs.61.5.24

Purpose. The axial separation between the iris and the intraocular lens (IOL) in pseudophakic eyes can cause rays originating from the far temporal field to miss the IOL, resulting in negative dysphotopsia (ND). We developed an experimental model to test the hypothesis that obstruction of rays from the far temporal field can generate ND and an accompanying loss of visual sensitivity in the far temporal field.

Methods. The right eyes of 10 phakic subjects were fitted with soft contact lenses containing a 5.50-mm central clear zone and a 12-mm outer diameter opaque annulus. In three of the subjects, eyes were dilated with 1% tropicamide solution, and effective aperture diameters were determined optically (pupil camera) and psychophysically (narrow beam detection). Visual field extent (Goldmann bowl) and temporal and inferotemporal meridian sensitivities (Octopus perimeter) were measured. A wide-angle model was constructed to quantify the impact of the annular opacity on retinal illuminance.

Results. All 10 subjects observed a dark crescent in the far temporal and inferotemporal fields. The opaque annulus reduced effective horizontal pupil diameters from 8 mm to 5.5 mm on-axis and from >2 mm to <1 mm at 90°. Perimetry revealed a 10° reduction in temporal and inferotemporal field extent and increasing loss of sensitivity beyond 70°. The wide-angle model confirmed significant vignetting (>50% beyond 70°), approaching zero retinal illuminance beyond 85°.

Conclusions. Vignetting of rays originating from the far temporal field by axially separated apertures can create symptoms mirroring perceptual reports of negative dysphotopsia in symptomatic pseudophakic patients.

Keywords: negative dysphotopsia, intraocular lens, vignetting, retinal illuminance, pseudophakia

Cataracts are the second leading cause of blindness and visual impairment worldwide, and they could affect 38 million people in the United States by 2030.[1,2] Over 3.6 million surgical cataract extractions are performed yearly in the United States.[3] Immediately after an uneventful cataract extraction and intraocular lens (IOL) implantation, about 15% of patients report seeing a dark shadow in their far temporal field, a form of visual field vignetting.[4] The cause of this negative dysphotopsia (ND) is unclear.[5,6] Persistent ND remains in 2% to 3% of patients (about 16,000 annually).

Evidence indicates that the dark shadow is created by reduced retinal illuminance in the far nasal retina because light from the far temporal field can miss the IOL and arrive anteriorly on the nasal retina or on the visually insensitive pars plana region of the ciliary body.[5–7] The posterior location and small size of typical IOLs have been implicated as the source of this far temporal field ND.[8,9] An absence of ND postoperatively has been attributed to axial separations between the iris and IOL being either too large or too small,[5,10,11] large pupils,[5,12] or insensitivity of the far nasal retina.[12,13] Its disappearance in most of the initially symptomatic eyes may reflect neural adaptation[14,15] or changes in IOL and/or iris location.[11,16] The larger phakic lens and the absence of any gap between the iris and phakic lens (Fig. 1A) ensure that even rays from the far temporal field are refracted by the lens and imaged onto the far nasal retina.[5,8]

Peripheral image vignetting is not unique to post-cataract surgery eyes. Prior clinical and modeling studies have reported a reduction of visual field extent in eyes wearing contact lenses with opaque peripheries.[17–19] Also, the opaque annular intracorneal inlay (KAMRA; CorneaGen, Seattle, WA, USA)[20] attenuates image ray intensities in the mid-peripheral visual field.[21,22] In pseudophakic eyes, vignetting of the peripheral retinal image is caused by incorrect imaging of the far temporal rays that have passed through the pupil (Fig. 1B), whereas in the corneal plane examples (contact lenses or corneal inlay) vignetting is due to an opacity preventing these rays from entering the anterior chamber (Fig. 1C). Both scenarios can produce reduced retinal illuminance in the far nasal retina, and in both cases the retinal location of the peripheral vignetting will be approximately stabilized because the optical causes (IOL, inlay, or contact lens) will move with the eye.

The goals of the current study were to develop an experimental model of far nasal retina vignetting and far temporal field ND in phakic eyes and to examine the relationship between ND and visual sensitivity. We developed a psychophysical ray tracing paradigm in order to make direct

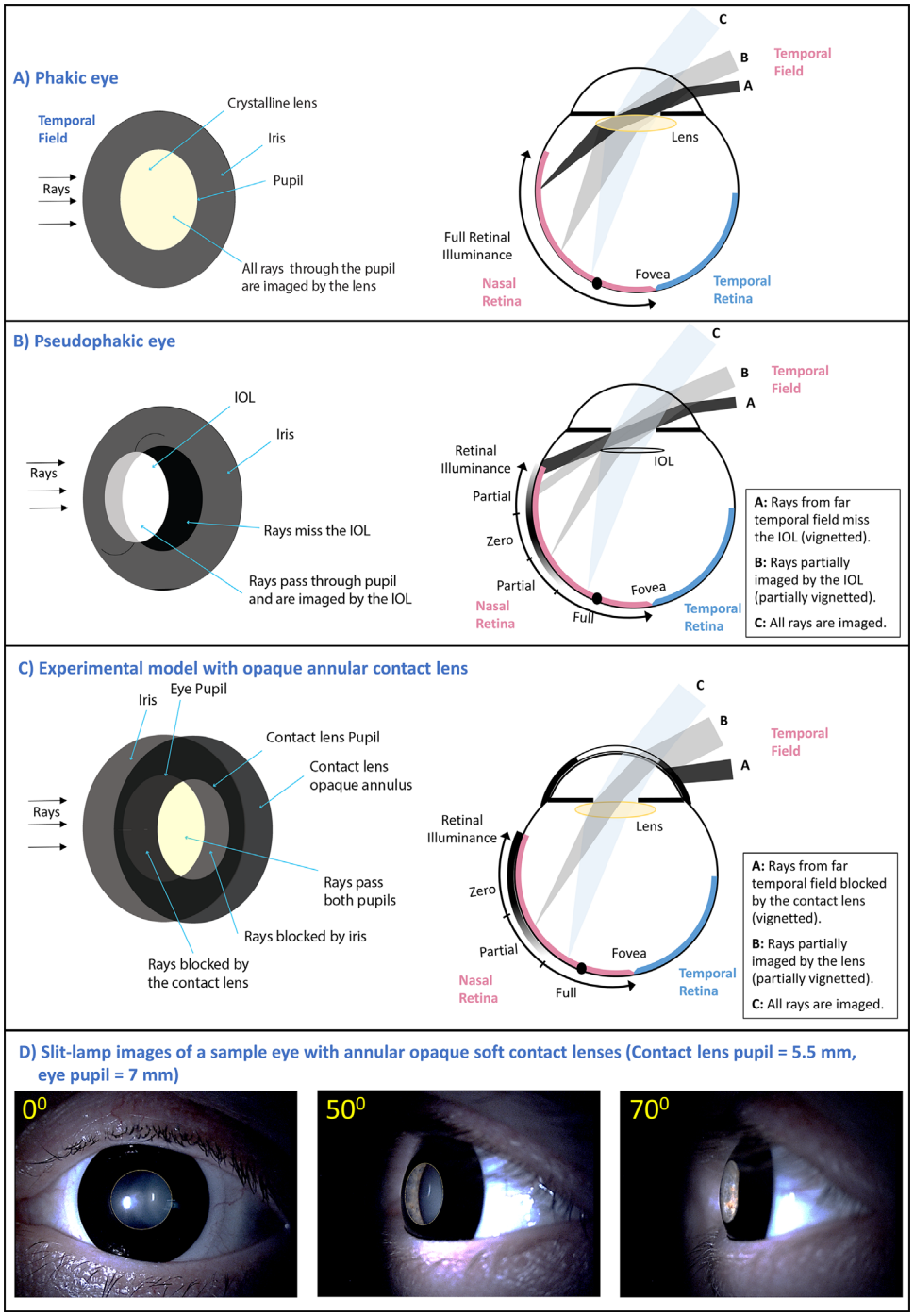

Figure 1. Schematic illustration of the iris and lens as viewed from the far temporal field (*left*) and the corresponding traces of far temporal ray bundles (*right*) in phakic (**A**), pseudophakic (**B**), and phakic eyes with the annular opaque contact lens (**C**). Notice that the two apertures (contact lens pupil and eye pupil) are laterally displaced (parallax effect) due to the axial separation between them. A sample eye with the opaque annular contact lens was imaged using a slit-lamp video system from different temporal angles after pupil dilation (**D**). The extent of the nasal and temporal retina was drawn based on histology data from the Curcio et al. study.[39]

comparisons with wide-angle model eye ray tracing. Wide-angle model eye ray tracing provided an accurate replication of the real eye psychophysical data.

Methods

Far Nasal Retina Vignetting in Pseudophakic Eyes

Rays entering the phakic eye from the far temporal field are imaged onto the far nasal retina (Fig. 1A, black rays), resulting in full retinal illuminance.[23] In the pseudophakic eye, due to the axial separation between the iris and IOL, some rays miss the IOL and arrive at a more anterior location of the nasal retina or ciliary body (Fig. 1B, gray and black rays). This anterior shift of the rays missing the IOL is reported to be between 10° and 15°.[24] Therefore, in pseudophakic eyes, regions of the far nasal retina may contain a mixture of rays that have missed the IOL and those that were imaged by the IOL.[5] The proportion of rays missing the IOL depends on the anterior chamber geometry and pupil size.[5,12] With

Investigative Ophthalmology & Visual Science

small pupils and typical axial separations between the iris and IOL, most of the temporal field rays (up to 70° or so) are imaged by the IOL, but a majority of rays originating from beyond 70° in the temporal field can miss the IOL.[5,12] For a narrow range of IOL and anterior chamber geometries (e.g., axial separations between 0.1 and 0.5 mm) and with small pupils (e.g., 2.5-mm diameter), rays that miss the IOL will be restricted to temporal field angles within 10° to 15° of the far edge of the field.[5] For this set of conditions, the far nasal retina will experience a large drop in retinal illuminance because the rays that miss the IOL will arrive anterior to the edge of the functional retina.[5,24] This causes an illumination gap on the far nasal retina which is a form of image vignetting that is perceived as a dark shadow by those patients experiencing ND. With large pupils and/or larger axial separations, rays that miss the IOL from smaller field angles illuminate the far nasal retina, preventing the formation of a dark shadow.[12,24]

Experimental Model of Far Nasal Retina Vignetting

As an experimental tool to investigate the perceptual consequences of reduced illumination in the far nasal retina, we created an experimental vignetting model using soft contact lenses. The soft contact lens had a clear central zone (5.5-mm diameter) surrounded by an opaque annulus (12-mm outer diameter), which is axially separated by the anterior chamber from the iris plane. Ray tracing a model phakic eye with this contact lens shows that the rays originating in the far temporal field were blocked from entering the iris pupil and thus reaching the far nasal retina (black rays in Fig. 1C). The opaque annulus in the contact lens, therefore, reduced retinal illuminance in the far nasal retina, mirroring the reduction in nasal retinal illuminance that causes ND in a subset of pseudophakic eyes. The pupil of a phakic eye fitted with this contact lens is partially occluded at field angles between 50° and 70° (Fig. 1D), resulting in decreased illuminance at the far nasal retina, which drops to zero beyond about 80° (see Fig. 8). The optical origins of vignetting of the nasal retinal image are, of course, different between the model and pseudophakic eyes. In pseudophakic eyes with small pupils, the far nasal retina is dark because rays arrive more anteriorly at the visually insensitive pars plana; whereas, in the experimental model, the far nasal retina is dark because rays do not pass through the pupil. Unlike the pseudophakic case, our model will create nasal retina vignetting with both small and large pupils. The axial separation of two apertures that are coaxial and appear concentric when viewed from the fixation point creates a parallax shift when viewed from a peripheral field angle, and when the two apertures are completely non-overlapping (at very high field angles) no light will enter the eye (Figs. 1C, 1D). Despite this difference, we believe the model provides important information about the origin of symptoms experienced by patients with ND.

Subjects

Ten healthy phakic subjects 22 to 62 years of age (mean ± SD: 33.8 ± 11.8 years) with no prior ocular surgery or disease were recruited. The mean ± SD spherical refractive error and photopic pupil size in the right eyes were –1.80 ± 2.66 D (range, +1.50 to –7.50 D) and 3.96 ± 0.48 mm (range, 3.10–4.70 mm), respectively. Right eyes were fitted with the opaque annular soft contact lens, and all subjects experienced the dark crescent in the far temporal and inferotemporal field mirroring the ND reported by symptomatic pseudophakes.[4,25] To investigate the visual consequence of far nasal vignetting with the experimental contact lens, a subset of three subjects (two males and one female; 62, 44, and 22 years of age) participated and signed an informed consent document. The study followed the tenets of the Declaration of Helsinki and was performed in accordance with an institutionally approved human subject protocol.

Pupils were dilated with 1% tropicamide to suppress unwanted accommodation, which it does effectively, but the primary intent was to introduce a stable mydriatic effect,[26] key to our experiments, and as such tropicamide is preferred over cyclopentolate. Dilated pupils provided the largest range of visible beam locations for the psychophysical ray tracing experiment (described below). After 30 minutes, dilated objective refraction was performed using a Grand Seiko autorefractor (WAM-5500; Shigiya Machinery Works Ltd., Hiroshima, Japan), and anterior segment was evaluated using slit-lamp biomicroscopy. The dilated spherical equivalent refractive errors of the subjects were +1.50 D, –2.50 D, and plano. Right eyes were fitted with opaque annular soft contact lenses containing the dilated spherical equivalent refraction. Soft contact lens assessment revealed well-centered fits in all subjects. With the left eye occluded, all testing was performed on the right eye with and without the opaque annular soft contact lenses.

Psychophysical Measurement of Vignetting

A custom psychophysical ray-tracing instrument (TTP: The Technology Partnership, Hertfordshire, UK) (Fig. 2) was used to measure the entrance pupil plane distribution of rays that reach the retina (and are therefore visible) and

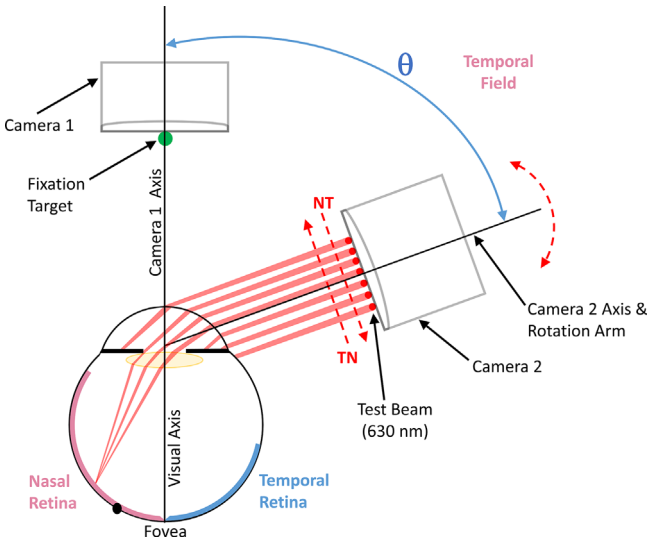

Figure 2. The psychophysical ray trace instrument with its components. The fixation target and Camera 1 are on a fixed arm coincident with the fixation target, whereas Camera 2 and the test beam are on a linear translation stage mounted on a rotation arm. For every rotation arm position, the test beam (*red*) was translated in 250-µm steps from the temporal to nasal limbus (TN), across the pupil, and back (NT), as shown by the *red dashed lines* with arrows.

those that fail to reach the retina (and are thus invisible). Easily visible stimuli (66-arcmin circles of 630-nm light) were displayed at temporal field eccentricities up to 90°. Projection optics were used to produce a narrow beam (0.55-mm diameter) that could be translated horizontally across the pupil in 250-µm steps, and an incremental rotary encoder manipulated the test beam entry angle. Subjects were asked to fixate a small green (540-nm) test light and press a trigger button whenever they saw the red (630-nm) test stimulus in the peripheral field. Two cameras, one fixed on the fixation axis (Camera 1) and the other on the rotation stage (Camera 2) were used to monitor eye position. A bite-bar on a XYZ motorized translation stage allowed stable and precise positioning of the eye. A custom MATLAB (MathWorks, Natick, MA, USA) program was used to acquire camera images, control test beam parameters (brightness, position, velocity), and read input from the trigger button. A detailed log of all instrument controls and subjects' psychophysical responses with time-stamps was recorded and saved as a .txt file.

Subjects were aligned to the instrument coordinate space using the XYZ translation stage, which brought the entrance pupil plane of the test eye to the focal planes of the cameras and into alignment with the center of rotation of the stage containing the test beam. This alignment was required to capture well-focused images of the eye and the test beam and to maintain the correct field angle of the test beam as it was rotated out from 0° to 90° in the temporal field. Neutral density filters with various attenuation levels (0.25 to 2.0 neutral density) were inserted in the test beam path to provide similar detectability (approximately 2 log units above threshold) of the test stimulus when displayed at different field angles. The test beam was translated horizontally from the temporal limbus, across the pupil, to the nasal limbus, and back in 250-µm steps. At each step, the test beam was turned on for 2 seconds, and the subject pressed the trigger button if the red stimulus was visible. Horizontal beam location and both horizontal and vertical pupil margins were continuously monitored and stored in order to correctly identify the actual beam entry position in the pupil plane. Detectability of the red test stimulus at each of up to 80 horizontal beam locations was assessed for beam entry angles of 4°, 50°, 60°, 70°, 80°, and 90° in the temporal visual field.

Offline analysis of the camera images (53 pixels/mm) required the user to load a video file and manually identify the location of the first Purkinje image, the test beam on the iris (when not passing through the pupil), and the nasal and temporal pupil margins on the first image. A 100 × 100-pixel region of interest around the marked Purkinje image was cropped to locate the center of the Purkinje image. The pupil center was calculated as the midpoint of the distance between the nasal and temporal pupil margins. Subsequent images were extracted from the video file with the same time-stamps as the psychophysical responses, and automated analysis was performed as follows: On each extracted image, a change in the Purkinje image position in the current image relative to the previous image revealed head (and therefore pupil) translations. From the pupil translation data, beam location was then remapped from instrument coordinates to pupil coordinates. Supplementary Videos S1 and S2 show the MATLAB image analysis of the video files from a subject for 4° and 80° test beam angles, respectively.

Visual Field Assessment

The extent of the right-eye visual field was measured using a Goldmann bowl perimeter displaying a size III stimulus with relative intensity of 4e. A skilled operator moved the target from the edge of the bowl (non-seeing area) toward the visual field center (seeing area) along each of the 24 meridians (0° to 345° in 15° increments) until the subject responded by pressing the clicker. The position of the first stimulus detection on the visual field was marked on a commercially available Goldmann scoring sheet. Two repeat measurements were performed in a random sequence along each meridian. In addition, subjects were asked to draw the extent and position of the perceived dark shadow on a Goldmann scoring sheet.

Visual field sensitivities in the right eye were measured using an Octopus 900 perimeter (Haag-Streit USA, Mason, OH, USA). Custom exams were created to measure sensitivities along two meridians at different eccentricities from the center: (1) horizontal (nasotemporal field), 70° nasal to 50° temporal in 10° steps, then 5° steps out to 90°; and (2) oblique (inferotemporal field, 330°): 10° to 30° in 10° steps, then 30° to 90° in 5° steps. Subjects fixated on a 0.43°-diameter spot and 10:00 position on a 5.4°-diameter ring while testing the nasotemporal and inferotemporal meridians, respectively. Luminance thresholds for detecting 100-ms presentations of size III white stimulus on a 31.4-apostilb white background were measured three times at each field eccentricity. The means and standard deviations for the sensitivities along the three meridians were calculated.

Ocular Biometry and Imaging

Three measurements of axial ocular biometry were performed using a LENSTAR LS 900 optical biometer (Haag-Streit USA). Anterior segment biometry was also acquired in the raw image mode using the anterior segment Visante OCT (Carl Zeiss Meditec, Jena, Germany).

Wide-Angle Optical Model of Negative Dysphotopsia

Wide-angle phakic eye models (four-surface) were constructed in sequential mode in OpticStudio 18.1 (Zemax, Kirkland, WA, USA) for the right eyes of each subject using the ocular biometry data. Briefly, images from the Visante OCT were corrected for distortions,[27] and spherical fits to the anterior and posterior corneal surfaces yielded radii of curvature. A single surface iris (aperture stop) with pupil diameter from Visante images was axially separated from the posterior corneal surface by the anterior chamber depth and iris thickness. Unaccommodated radii of curvature of the anterior and posterior crystalline lens surfaces, lens equatorial diameter, and lens equivalent refractive index were calculated for each subject using the age-dependent biometry relationships from prior studies.[28–30] Refractive indices of ocular media from the Gullstrand eye model were used.[31] The lens equivalent refractive index was optimized in OpticStudio to match the model eye refraction to the WAM-5500-measured dilated spherical equivalent refraction. A single surface contact lens with a 5.5-mm-diameter clear central optic zone and 12-mm-diameter opaque annulus containing the dilated spherical equivalent refractive correction was located on the front of the cornea. The contact lens and the anterior corneal surface were separated by a central

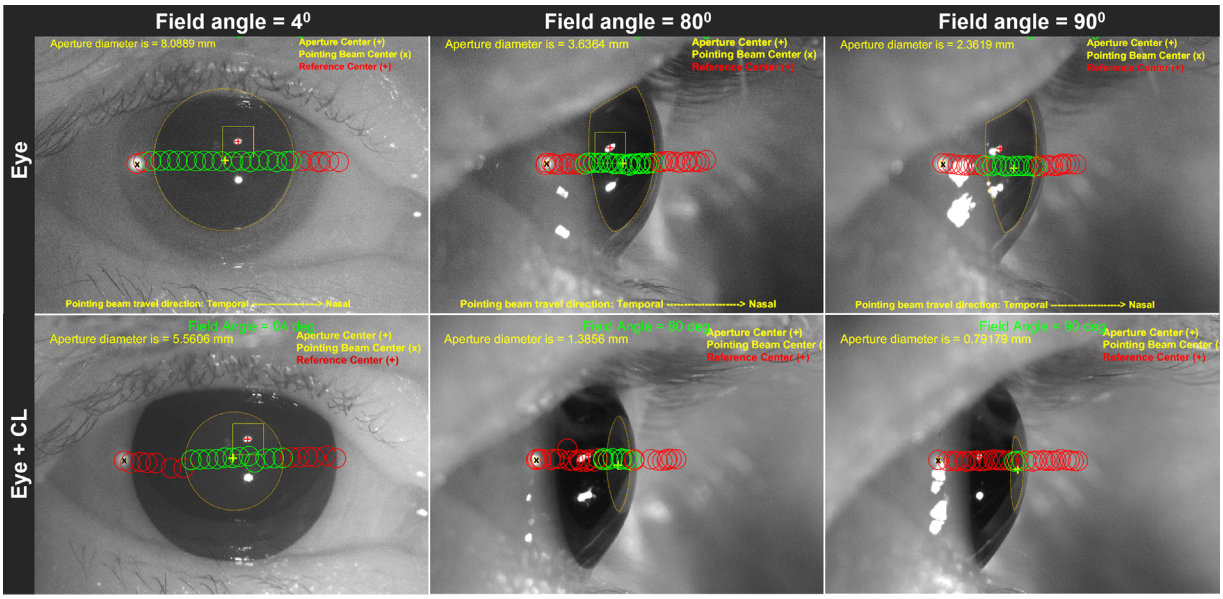

Figure 3. Sample data from a subject showing effective test beam positions with psychophysical responses (seen, *green circles*; not seen, *red circles*) for three field angles with and without the contact lens. Eye (and pupil) positions were monitored and marked at each frame to calculate effective beam positions. Effective aperture (pupil) edge, *yellow dotted lines*; aperture center, *yellow cross*; Purkinje image position, *red cross with yellow search box*; initial test beam position, *black x*. Off-axis pupil determination employed user-directed fitting of ellipses and examination of the video stream to reject false aperture boundaries created by internal system reflections (e.g., second low-contrast image that is ~2 mm above the primary image in each panel).

contact lens thickness measured using a thickness gauge (Createch/Rehder-dev Co, Chesterfield Township, MI, USA). A spherical retina (–12-mm radius) was located behind the anterior corneal surface by the measure of axial length.

For each subject, models were constructed with and without the annular contact lens. In each eye model, object rays from 0° (visual axis) to up to 90° in 1° steps in the temporal visual field (22,701 rays/field angle) were traced. For each field angle, we first quantified the proportion of image rays that reached the retina (unvignetted) to the total object rays at the entrance pupil plane of the model. For example, in the eye alone model, all rays that pass through the entrance pupil reach the retina (assume 100% transparency). However, in the eye + contact lens model, the contact lens aperture becomes the entrance pupil, and with increasing field angle rays that pass through the contact lens pupil can fail to pass through the iris pupil, reducing the proportion of rays reaching the retina. Second, to quantify the visual impact of vignetted rays on the retinal image, relative illuminance at each nasal retina eccentricity (retinal field angle subtended at the secondary nodal point) was calculated in OpticStudio by integrating rays across the exit pupil that arrive at each retinal location. With this second metric, factors such as off-axis aberrations and distance from the iris to the retina also contribute to the final retinal illuminance.

Results

Sample pupil images, beam locations (circles), and visibility data (red or green) observed with and without the annular opaque contact lens for three field angles are shown in Figure 3. The effective horizontal pupil diameter of the phakic eye was reduced with the annular opaque contact lens for all field angles, and the eye pupil and the contact lens pupil became elliptical for large field angles due the approximate cosine compression of the two apertures.[32] Also, because of the axial separation of the contact lens and eye entrance pupils, the effective pupil is limited by the temporal edge of the contact lens pupil and the nasal edge of the eye pupil, thereby reducing the effective horizontal aperture diameter.

Sample psychophysical responses from a subject with and without the annular opaque contact lens for the 80° field angle are shown in Figure 4A. The range of beam positions (x-axis) where the beam was visible ($P = 1$) was reduced with the contact lens (orange lines), in agreement with the measured pupil image (dashed lines). Effective horizontal aperture diameter was calculated from the psychophysical responses for the beam visible 50% of time by calculating the average range of pointing beam positions (x-axis) where the beam was seen ($P = 1$) and not seen ($P = 0$). For all field angles, the aperture diameters (calculated from the images (Fig. 3) and psychophysical responses (Fig. 4A) were reduced with the aperture contact lenses compared to the eye alone in all three subjects (Figs. 4B–4D). The effective aperture diameters from the psychophysical responses with and without the annular contact lens were slightly larger than those measured directly from the images for most field angles because of the finite size of the test beam (0.55-mm diameter) and the variability associated with the detection criteria used by subjects. These results establish that rays passing through each point across the effective pupil diameter can be detected in the far peripheral retina in spite of reduced sensitivity[13] and elevated optical aberrations.[33]

Consistent with the vignetting model (Fig. 1), Goldmann bowl results showed approximately 10° reductions in the horizontal, inferotemporal, and superotemporal visual fields in all three subjects with the opaque annular contact lenses (Figs. 5A, 5C, 5E). No significant reduction in the inferior, superior, and nasal field extent was observed. Consistent

Investigative Ophthalmology & Visual Science

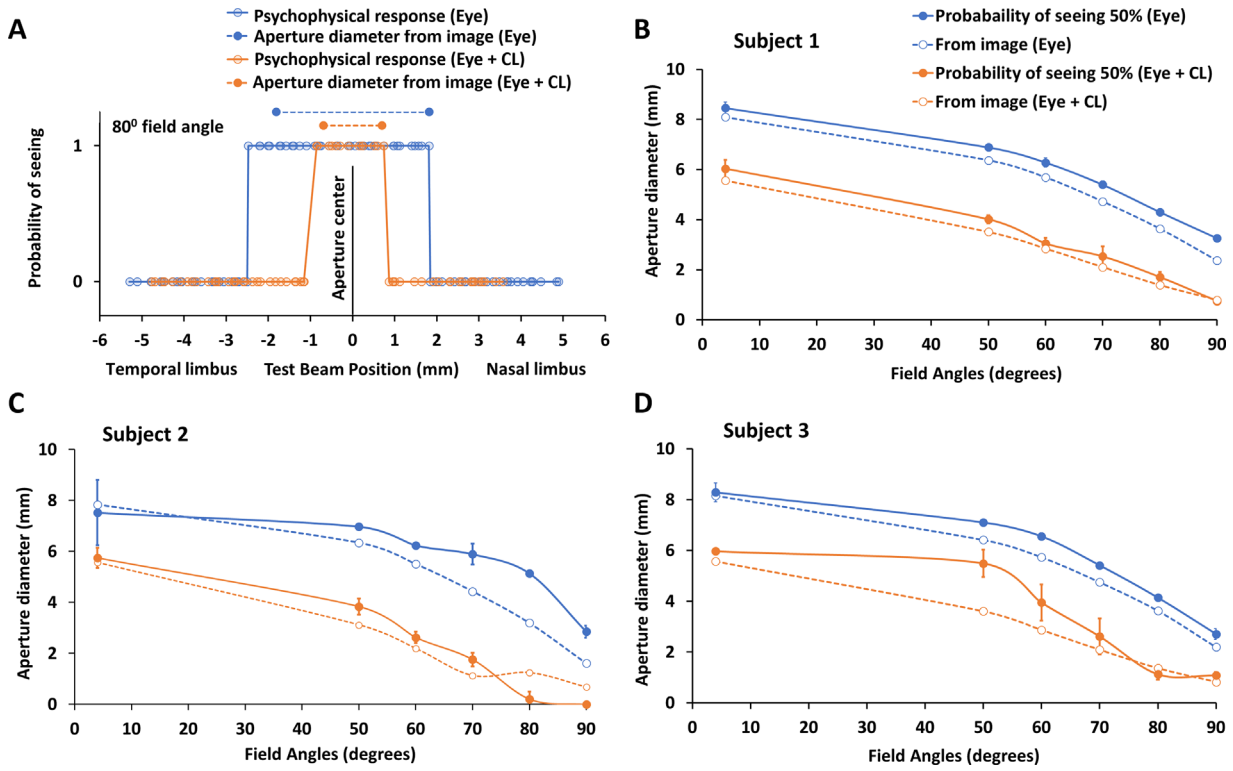

Figure 4. Sample psychophysical responses from the analyzed video frames (Fig. 3) from a subject with and without the contact lens (**A**). Responses from both test beam translations (temporal to nasal and back) were combined and plotted as a function of test beam positions at the eye plane. All subjects had reduced apertures with the contact lenses indicating vignetting from the opaque annulus of the contact lens (**B–D**). *Error bars* represent standard deviations from two measurements. Dashed lines above the psychophysical data show the pupil aperture size and location determined from camera images that were captured at each field location.

with the Goldmann data, subjects reported seeing dark shadows only in the temporal and inferotemporal fields with the annular opaque contact lens (see the drawings made by each subject in Figs. 5B, 5D, 5F). Inter-subject differences in the perception of the dark shadow are anticipated because of eye-specific anterior segment biometry and contact lens position.

Peripheral field light sensitivity data from individual subjects (Figs. 6A–6F) and mean data (Figs. 6G, 6H) reveal almost no effect of the contact lens on visual sensitivity for field angles < 70°. However, there was significant reduction in light sensitivity in the far temporal and inferotemporal fields and an inability to detect light beyond about 80°, which corresponds to both the field reductions observed in the Goldmann bowl and the subject drawings of their negative dysphotopsias (Fig. 5). Reductions in light sensitivity > 2 standard deviations of measurement error (shown in gray) were observed at field angles larger than 70°.

The optical model of a sample eye without the contact lens (Fig. 7A) revealed full illumination of the pupil with rays originating from central and peripheral visual field locations (including 90°, red rays). The proportion of the pupil transmitting rays to the retina was quantified as the proportion of unvignetted rays in Figure 8A (black circles), which was 1.0 for the eye alone at all field angles. With the annular opaque contact lens on the cornea, the available aperture diameter was reduced to 5.50 mm. The same model with the annular contact lens (Fig. 7B) showed that along the optical and visual axes of the eye (Fig. 7B, blue and green rays) all rays that passed the contact lens aperture also passed through the iris aperture (8-mm diameter). Out to approximately 45° (Fig. 7B, yellow rays), all rays that passed through the contact lens pupil also passed through the iris pupil. However, beyond 45° in the temporal field, an increasing proportion of the rays passing through the contact lens pupil arrived at the nasal iris and were not transmitted to the retina. Additionally, rays from the far temporal field beyond 80° (Fig. 7B, red rays; Fig. 8A, colored circles) that would have passed through the iris pupil (Fig. 7A) were completely obstructed by the opaque contact lens annulus (Fig. 7B). Figure 8A quantifies this change by plotting the proportion of rays passing through the contact lens aperture that also passed the iris aperture as unvignetted rays.

The visual consequence of on- and off-axis ray transmission can be described by the relative retinal illumination metric. In the eye alone condition, the model revealed full retinal illuminance (≥1.0) (Fig. 8B, colored diamonds), mirroring the 100% ray transmission data from Figure 8A (black circles) combined with reduced distance from the pupil to the retina.[23] With the eye + contact lens condition, full retinal illuminance was observed (Fig. 8B, colored circles) up to 45° due to full ray transmission (Fig. 8A, colored circles). Beyond 45°, retinal illuminance declined due to partial obstruction by the opaque annulus, leading to zero retinal illuminance beyond 80° due to total obstruction of far temporal rays. The optical model estimates of the proportion of unvignetted rays and retinal illumination were strongly correlated but non-linearly (Fig. 8C). Several factors affect the impact of stimulus location in the visual field on retinal illuminance (but not on proportion of

Investigative Ophthalmology & Visual Science

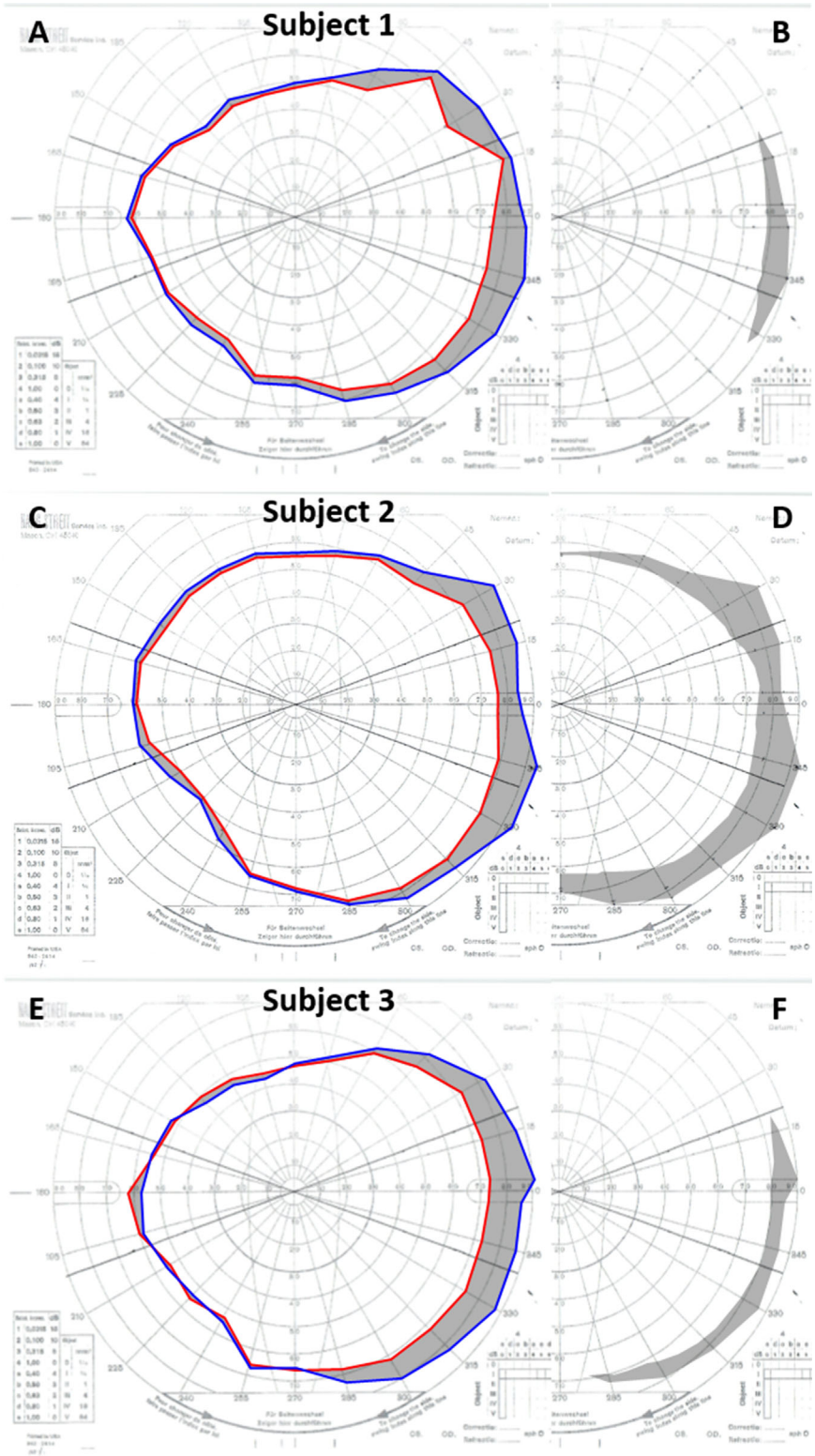

Figure 5. Goldmann bowl traces of visual field extent with a III4e stimulus for the eye (*blue*) and eye + contact lens (*red*) (**A**, **C**, **E**). The *gray area* between the *red* and *blue traces* indicates the visual field loss with the annular opaque contact lens. Subjects also reported seeing the dark shadow (*gray area*) with the annular contact lens (**B**, **D**, **F**).

unvignetted rays), including elevated off-axis aberrations,[33] cosine compression of the pupil,[32] and change in distance of the retina from the pupil.[23] For the optical model, total far temporal ray obstruction and total loss of retinal illumination with the contact lens were observed for rays beyond 80° (Figs. 8A, 8B, red dashed arrows) and this agreed well

Investigative Ophthalmology & Visual Science

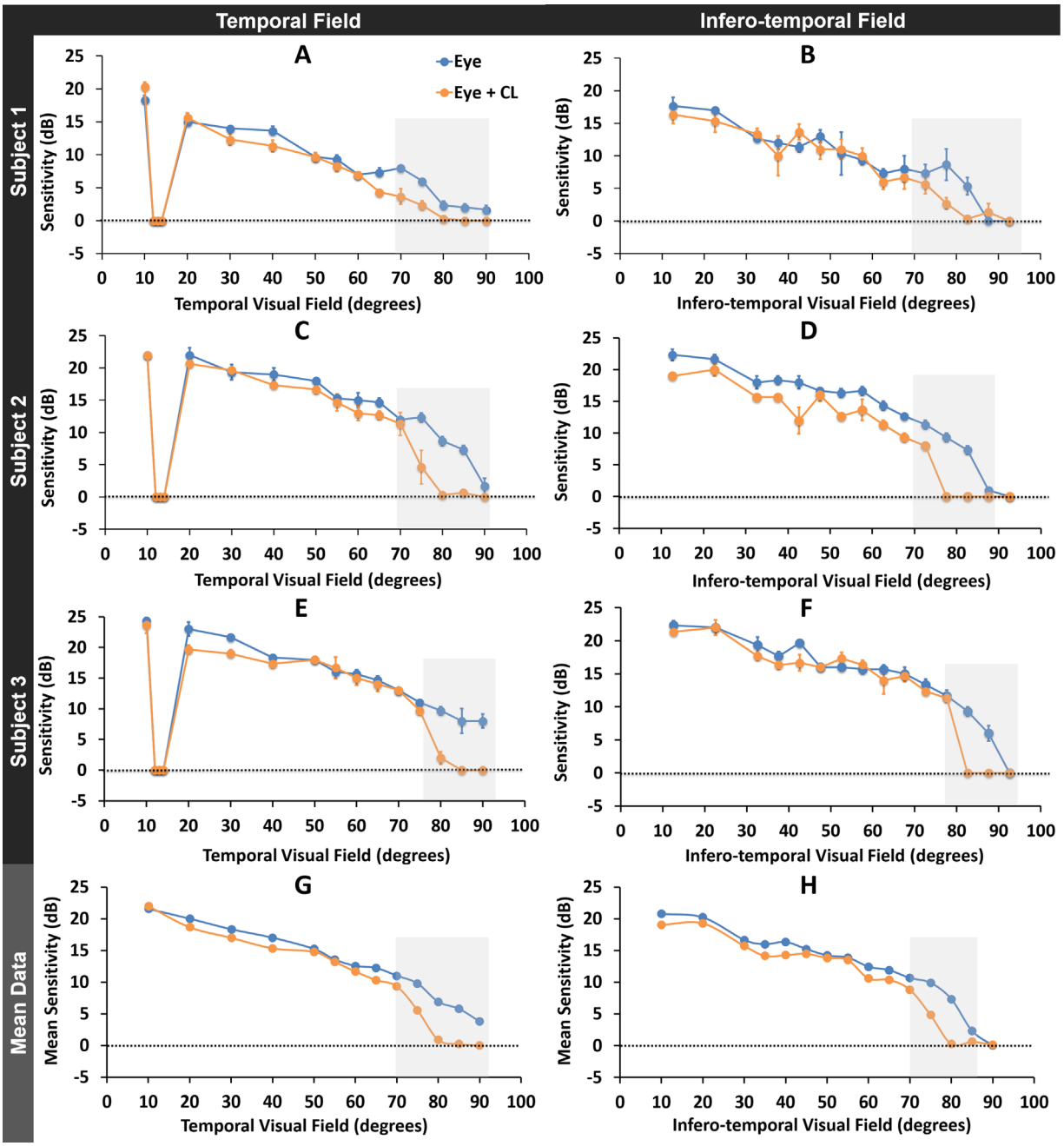

Figure 6. Visual sensitivity along the temporal (**A–C**) and inferotemporal (**D–F**) meridians from individual subjects and group mean (**G**, **H**) with and without contact lenses from the Octopus perimeter. All subjects had sensitivity loss beyond 80° and reduced sensitivities (*gray box*) in several field locations with the annular opaque contact lens. *Error bars* represent standard errors of the mean from three repeat measurements.

with the data from Goldmann (Fig. 5, red trace) and Octopus perimeter (Fig. 8D, red dashed arrows).

Discussion

The experimental model of negative dysphotopsia using opaque annular contact lenses obstructed rays originating from the far temporal and inferotemporal fields creating the far temporal dark shadow in phakic eyes similar to that seen by post-cataract surgery patients that are symptomatic of ND. The subject drawings of the simulated ND (Fig. 5) were comparable to drawings by pseudophakic subjects who experience ND.[4,25,34,35] The subjective experience of simulated ND was present in the same field directions as the observed reduced sensitivity to light (Figs. 5, 6) and the compression of the horizontal extent of the pupil (Fig. 4). These observations confirm that this perceptual phenomenon can be caused by vignetting of far temporal field rays, consistent with a key hypothesis to explain ND in post-cataract surgery eyes. These results also explain the field loss associated with contact lenses or corneal inlays that employ opaque surrounds.[17,18,21] Ray tracing models

Investigative Ophthalmology & Visual Science

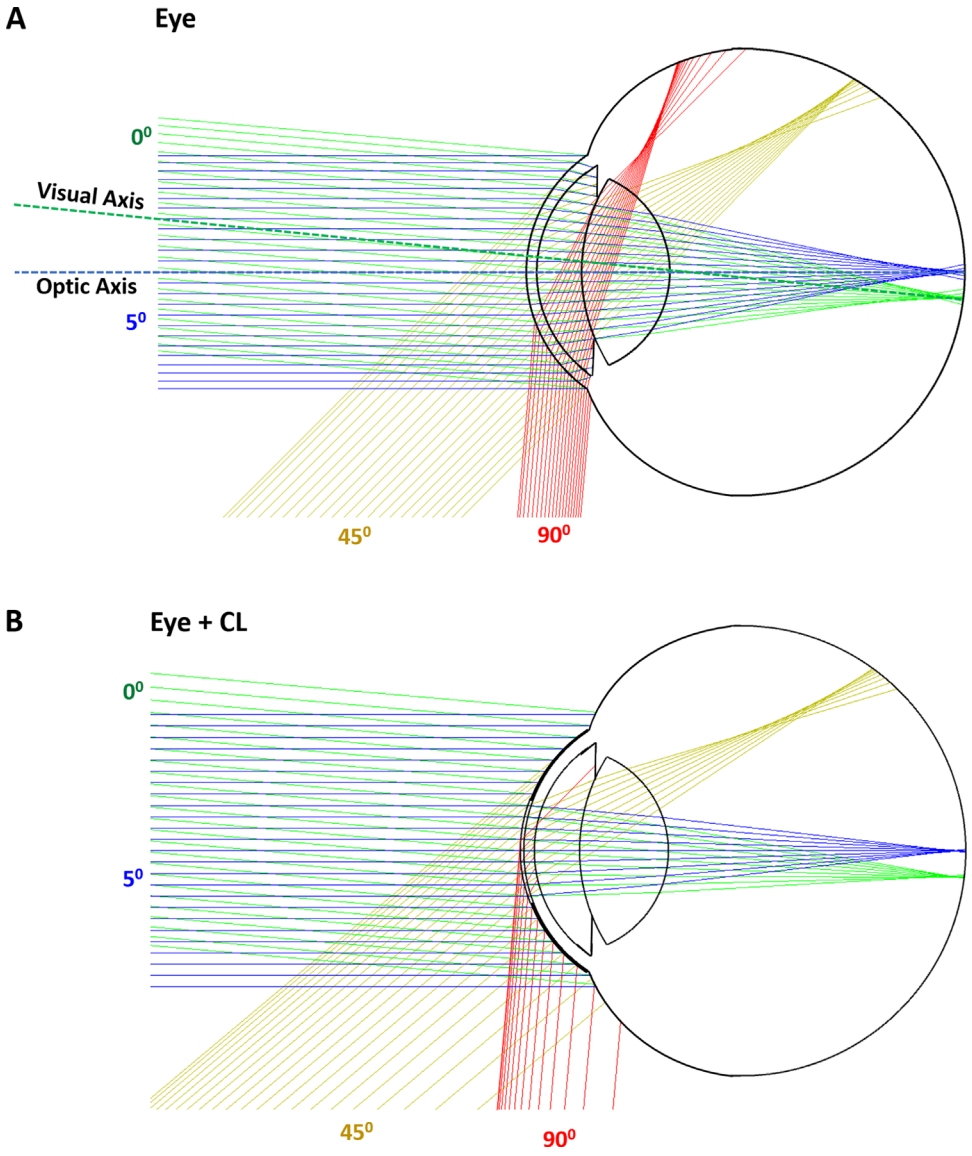

Figure 7. Optical model of a sample eye (subject 1) with no contact lens (**A**) and with the annular opaque contact lens (**B**). This eye was hyperopic, and the limiting aperture (7.58-mm eye pupil) was completely filled with on- and off-axis rays, resulting in 100% transmission (**A**). With the annular contact lens, the effective aperture was reduced to 5.50 mm, where rays in *yellow* were partially blocked by the opaque annulus. Notice that for the far temporal rays (90°; *red*) most rays were completely blocked by the contact lens; the few that made it through the contact lens were either totally internally reflected due to the high angle of incidence or blocked by the nasal iris (**B**).

of ND reveal that small differences in the location of far temporal field dark shadows are anticipated in our phakic model of ND because of eye-specific anterior segment biometry and contact lens positions. Likewise, eye-specific geometry in pseudophakic eyes (e.g., IOL and iris axial positions, anterior chamber depth) predicts the presence and location of dark shadows in the far nasal retina.[5,16,36]

Reductions in visual sensitivity with increasing angles in the far temporal field (Fig. 6) are due to optical and neural factors. By plotting the ratio of sensitivities observed with and without the contact lens in place (Fig. 8D), we were able to isolate the impact of optical vignetting. The dramatic drop in visual sensitivity at 80° (Fig. 8D) caused by vignetting contrasts with the optical model predicted reductions in nasal retinal illumination for field angles beyond 45° (Fig. 8B). Reductions in retinal illuminance caused by vignetting equally attenuate both the stimulus luminance (ΔL) and the background luminance (L) during visual field testing, maintaining stimulus contrast. The 50% reduction in retinal illuminance between 45° and 70° (Fig. 8B) reduces the perimeter background luminance from 31.4 to 15.7 apostilbs, or 10 to 5 cd/m^2, and also lowers the test probe luminance by the same factor, which would result in no change in detectability as long as Weber's law is applied ($\Delta L/L = K$). Aulhorn et al.[13] measured stimulus thresholds for several background luminances in the nasal visual field, revealing approximate Weber's law behavior at stimulus luminances similar to those employed in the Octopus perimeter (3–4000 apostilbs). Beyond 80°, the opaque annulus attenuated 100% of the light, consistent with the abrupt drop in visual sensitivity beyond 70° and complete failure to detect at eccentricities of ≥80°. As the effective background lumi-

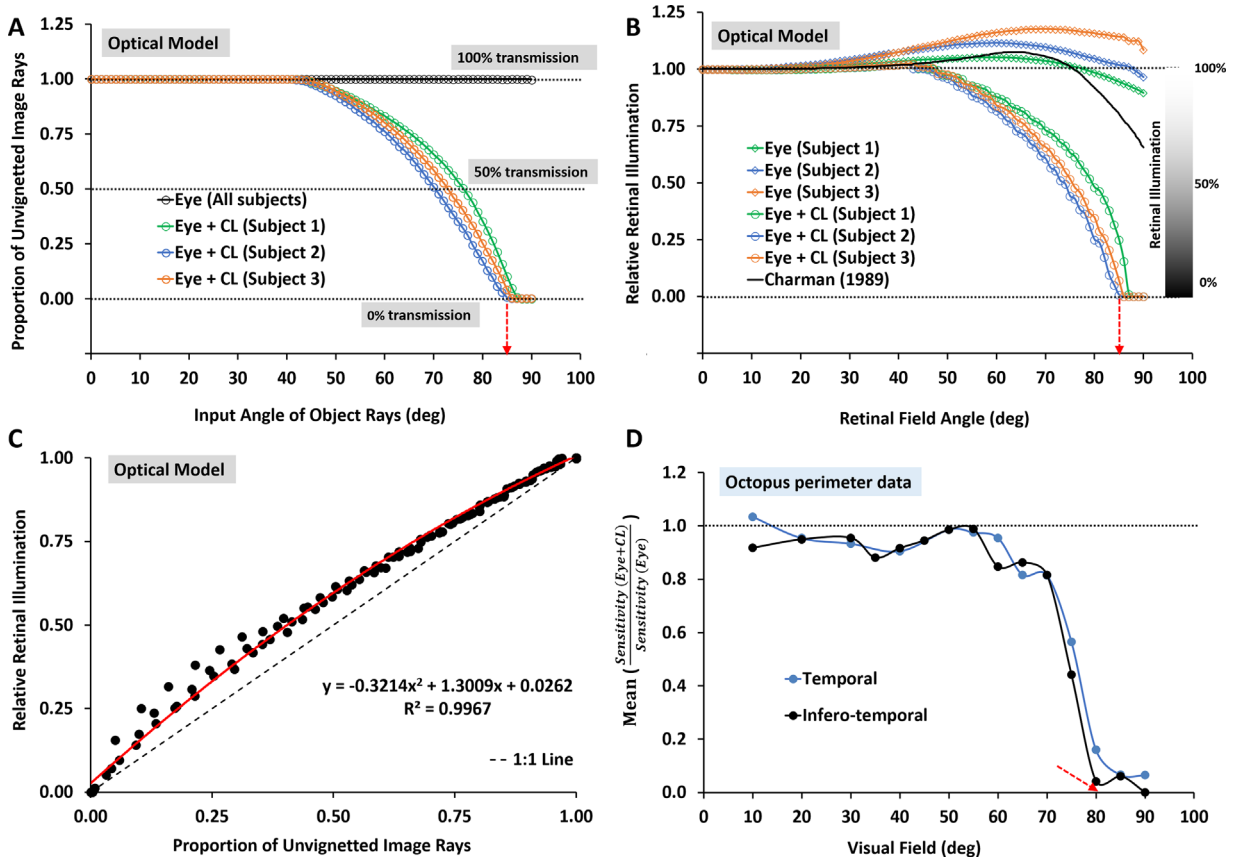

Figure 8. Optical model estimates of the proportion of rays unvignetted (transmitted) (**A**) and the resulting illumination at the retina (**B**) with and without the contact lens from the three subjects. Retinal field angle refers to the angular location on the retina corresponding to visual field location in the object space. *Red dashed lines* with arrows show the limit of the temporal visual field with the contact lens where there was zero ray transmission and zero retinal illumination. (**C**) Non-linear relationship between the proportion of transmitted rays and relative retinal illumination from all subjects. (**D**) Mean proportion of sensitivity loss (Octopus data, ratio of thresholds with and without the contact lens) across the temporal visual field. Significant reduction in light sensitivity was observed beyond 70°, with a total loss of light detectability beyond 80°.

nance dropped below 5 cd/m^2 at eccentricities > 70°, visual sensitivity decreased with decreasing retinal illuminance (as expected from the square root law, which manifests at lower photopic and mesopic light levels[13,37]), eventually making the maximum contrast test in the perimeter invisible. Consistent with the optical model by Holladay and Simpson,[5] our results emphasize that reductions in nasal retinal illuminance likely exist at smaller field angles than the measured field loss.[25]

The opaque annular contact lens used in this experimental model acted as a field stop, much like placing a pinhole in front of the eye. The result was reduced visual field extent due to the aperture size and axial position of the field stop, as well as the optical system behind the field stop—in this case, the eye. This finding, predicted by geometric optics, was supported by confirmation of the presence of a dark crescent in the far temporal and inferotemporal fields by all 10 subjects. Differences in eye/contact lens models could be introduced by changing the contact lens aperture, choosing eyes with varying anterior chamber depths, changing iris pupils, and selecting eyes with different vitreal chamber structures. However, due to the great challenges of collecting reliable psychophysical data at such large field angles, we concentrated on detailed data collection for a few eyes. As such, we failed to employ between-eye variability as a tool to understand the presence or absence of ND, which is a future project. The similarity of the detailed results of three subjects and the uniformity of the experience of our 10 subjects indicate that our approach is a reliable tool for generating far temporal field ND in the presence of the typical variability of ocular structures in normal healthy eyes.

Our experimental model emphasizes the ability of ray tracing to capture the key optical and retinal factors contributing to ND,[5,12] consistent with the hypothesis that the axial separation between the IOL and iris is the primary cause of ND in pseudophakic eyes.[5,12] As shown in Figure 4 of the Holladay and Simpson paper,[5] the field angle over which rays fail to be imaged by the IOL and the presence of ND can be reduced by placing the IOL closer to the iris. For example, strategies such as reverse optic capture[38] and implanting a piggyback IOL in the ciliary sulcus[24] to move the IOL refractive surface closer to the iris have been successfully employed to resolve persistent ND. Patient education in all individuals undergoing surgery regarding the potential for short- or long-term ND is also prudent, so patients know what to expect. The opaque annular contact lens used in the current study provides a simple experimental model in which far temporal field ND can be induced and is a valuable tool for exploring neural adapta-

tion to ND without the complicating factors of changing iris and IOL locations.

Acknowledgments

The authors thank members of the Clinical Optics Research Lab at the Indiana University School of Optometry for their help in collecting the clinical data and for their useful insights into the data analysis. We also thank Luis-Diaz Santana (TPP: The Technology Partnership, Hertfordshire, UK) and the research team at Alcon (Ft. Worth, TX, USA), especially Victor Hernandez, for their support with the psychophysical ray-tracing instrument.

Supported in part by Alcon.

Disclosure: **V. Ramasubramanian**, None; **D. Meyer**, None; **P.S. Kollbaum**, None; **A. Bradley**, Alcon (C)

References

1. National Eye Institute. Cataract data and statistics: cataracts defined. Available at: https://www.nei.nih.gov/learn-about-eye-health/resources-for-health-educators/eye-health-data-and-statistics/cataract-data-and-statistics. Accessed April 29, 2020.
2. World Health Organization. Blindness and vision impairment. Available at: https://www.who.int/news-room/fact-sheets/detail/blindness-and-visual-impairment. Accessed April 29, 2020.
3. Lindstrom R. Thoughts on cataract surgery: 2015. *Rev Ophthalmol*. 2015. Available at: https://www.reviewofophthalmology.com/article/thoughts-on–cataract-surgery-2015. Accessed April 29, 2020.
4. Osher RH. Negative dysphotopsia: long-term study and possible explanation for transient symptoms. *J Cataract Refract Surg*. 2008;34:1699–1707.
5. Holladay JT, Simpson MJ. Negative dysphotopsia: causes and rationale for prevention and treatment. *J Cataract Refract Surg*. 2017;43:263–275.
6. Holladay JT, Zhao H, Reisin CR. Negative dysphotopsia: the enigmatic penumbra. *J Cataract Refract Surg*. 2012;38:1251–1265.
7. Simpson MJ. Double image in far peripheral vision of pseudophakic eye as source of negative dysphotopsia. *J Opt Soc Am A Opt Image Sci Vis*. 2014;31:2642–2649.
8. Simpson MJ. Managing and understanding negative dysphotopsia. *J Cataract Refract Surg*. 2015;41:477.
9. Erie JC, Simpson MJ, Bandhauer MH. A modified intraocular lens design to reduce negative dysphotopsia. *J Cataract Refract Surg*. 2019;5:1013–1019.
10. Pereira FA, Cronemberger S. Ultrasound biomicroscopic study of anterior segment changes after phacoemulsification and foldable intraocular lens implantation. *Ophthalmology*. 2003;110:1799–1806.
11. Muzyka-Wozniak M, Ogar A. Anterior chamber depth and iris and lens position before and after phacoemulsification in eyes with a short or long axial length. *J Cataract Refract Surg*. 2016;42:563–568.
12. Simpson MJ. Vignetting and negative dysphotopsia with intraocular lenses in "far peripheral vision". *J Opt Soc Am A Opt Image Sci Vis*. 2015;32:1672–1677.
13. Aulhorn E, Harms, H. Visual perimetry. In: Jameson D, Hurvich LM , eds. *Visual Psychophysics*. Berlin: Springer-Verlag; 1972:102–145.
14. Rosa AM, Miranda AC, Patricio M, et al. Functional magnetic resonance imaging to assess the neurobehavioral impact of dysphotopsia with multifocal intraocular lenses. *Ophthalmology*. 2017;124:1280–1289.
15. Coroneo M. Cataract surgical problem. *J Cataract Refract Surg*. 2005;31:652–653.
16. Simpson MJ, Muzyka-Wozniak M. Iris characteristics affecting far peripheral vision and negative dysphotopsia. *J Cataract Refract Surg*. 2018;44:459–465.
17. Josephson JE, Caffery BE. Visual field loss with colored hydrogel lenses. *Am J Optom Physiol Opt*. 1987;64:38–40.
18. Lee DY, Jurkus JM, Ma S. Effect of the opaque, colored dot-matrix contact lens on visual field. *Int Contact Lens Clin*. 1990;17:188–191.
19. Carkeet A. Field restriction and vignetting in contact lenses with opaque peripheries. *Clin Exp Optom*. 1998;81:151–158.
20. Naroo SA, Bilkhu PS. Clinical utility of the KAMRA corneal inlay. *Clin Ophthalmol*. 2016;10:913–919.
21. Langenbucher A, Goebels S, Szentmary N, Seitz B, Eppig T. Vignetting and field of view with the KAMRA corneal inlay. *Biomed Res Int*. 2013;2013:154593.
22. Atchison DA, Blazaki S, Suheimat M, Plainis S, Charman WN. Do small-aperture presbyopic corrections influence the visual field? *Ophthalmic Physiol Opt*. 2016;36:51–59.
23. Charman WN. Light on the peripheral retina. *Ophthalmic Physiol Opt*. 1989;9:91–92.
24. Erie JC, Simpson MJ, Bandhauer MH. Effect of a sulcus-fixated piggyback intraocular lens on negative dysphotopsia: ray-tracing analysis. *J Cataract Refract Surg*. 2019;45:443–450.
25. Makhotkina NY, Berendschot TT, Nuijts RM. Objective evaluation of negative dysphotopsia with Goldmann kinetic perimetry. *J Cataract Refract Surg*. 2016;42:1626–1633.
26. Marchini G, Babighian S, Tosi R, Perfetti S, Bonomi L. Comparative study of the effects of 2% ibopamine, 10% phenylephrine, and 1% tropicamide on the anterior segment. *Invest Ophthalmol Vis Sci*. 2003;44:281–289.
27. Ramasubramanian V, Glasser A. Distortion correction of visante optical coherence tomography cornea images. *Optom Vis Sci*. 2015;92:1170–1181.
28. Dubbelman M, Van der Heijde GL. The shape of the aging human lens: curvature, equivalent refractive index and the lens paradox. *Vision Res*. 2001;41:1867–1877.
29. Rozema JJ, Atchison DA, Kasthurirangan S, Pope JM, Tassignon MJ. Methods to estimate the size and shape of the unaccommodated crystalline lens in vivo. *Invest Ophthalmol Vis Sci*. 2012;53:2533–2540.
30. Strenk SA, Semmlow JL, Strenk LM, Munoz P, Gronlund-Jacob J, DeMarco JK. Age-related changes in human ciliary muscle and lens: a magnetic resonance imaging study. *Invest Ophthalmol Vis Sci*. 1999;40:1162–1169.
31. Gullstrand A, von Kries J, Nagel W. *Handbuch der physiologischen Optik*. Hamburg, Germany: Verlag von Leopold Voss; 1909:382–415.
32. Mathur A, Gehrmann J, Atchison DA. Pupil shape as viewed along the horizontal visual field. *J Vis*. 2013;13:1–8.
33. Atchison DA, Scott DH. Monochromatic aberrations of human eyes in the horizontal visual field. *J Opt Soc Am A Opt Image Sci Vis*. 2002;19:2180–2184.
34. Vamosi P, Csakany B, Nemeth J. Intraocular lens exchange in patients with negative dysphotopsia symptoms. *J Cataract Refract Surg*. 2010;36:418–424.
35. Trattler WB, Whitsett JC, Simone PA. Negative dysphotopsia after intraocular lens implantation irrespective of design and material. *J Cataract Refract Surg*. 2005;31:841–845.
36. Simpson MJ. Intraocular lens far peripheral vision: image detail and negative dysphotopsia. *J Cataract Refract Surg*. 2020;46:451–458.

Investigative Ophthalmology & Visual Science

37. Van Nes FL, Bouman MA. Spatial modulation transfer in the human eye. *J Opt Soc Am*. 1967;57:401–406.
38. Masket S, Fram NR, Cho A, Park I, Pham D. Surgical management of negative dysphotopsia. *J Cataract Refract Surg*. 2018;44:6–16.
39. Curcio CA, Allen KA. Topography of ganglion cells in human retina. *J Comp Neurol*. 1990;300:5–25.

Supplementary Material

Supplementary Video S1. Sample image analysis of a video sequence from a subject without the contact lens. The test beam is 4° temporal to the visual axis. In each frame, the Purkinje image center with the search box (red cross and yellow box), pupil center (yellow cross), and initial test beam position (red circle with yellow x) are monitored and plotted. When the test beam is horizontally translated, notice that the subject initially does not see the beam (red circles) but then the beam is visible (green circles) across the pupil and is again not seen, as we expected. Subject responses of beam visibility were consistent in the return path, as well. For clarity, the test beam is shown to translate in 500-µm steps, and all beam positions (red/green circles) are plotted on the first frame after correcting for eye movements.

Supplementary Video S2. Analyzed video sequence from the same subject as in Supplementary Video S1 showing test beam positions arriving from 80° temporal to the visual axis. For far temporal rays, notice that the effective entrance pupil aperture is reduced horizontally, resulting in an elliptical pupil. The temporal pupil edge is indistinct due to the topography of the peripheral cornea and limbus.

Investigative Ophthalmology & Visual Science